# We are IntechOpen, the world's leading publisher of Open Access books Built by scientists, for scientists

6,900
Open access books available

185,000
International authors and editors

200M
Downloads

Our authors are among the

154
Countries delivered to

TOP 1%
most cited scientists

12.2%
Contributors from top 500 universities




WEB OF SCIENCE™

Selection of our books indexed in the Book Citation Index in Web of Science™ Core Collection (BKCI)

## Interested in publishing with us?
## Contact book.department@intechopen.com

Numbers displayed above are based on latest data collected.
For more information visit www.intechopen.com



Chapter 4

# The Heat and Mass Transfer Analysis During Bunch Coating of a Stretching Cylinder by Casson Fluid

Taza Gul and Shakeela Afridi

Additional information is available at the end of the chapter

http://dx.doi.org/10.5772/intechopen.79772

**Abstract**

The aim of this study is to coat a stretching cylinder with the help of a liquid film spray. The Casson fluid has been chosen for the coating phenomena. The thickness of the liquid film has been used as variable, and the influence of heat and mass transmission under the impact of thermophoresis has been encountered in the flow field. The required pressure term for the spray pattern during variable thickness has mainly been focused. Using the suitable similarity transformations, the basic flow equations for the fluid motion have been converted into high-order nonlinear coupled differential equations. Series solutions of subsequent problem have been obtained using controlling procedure optimal approach. Important physical constraints of skin friction, Nusselt number, and Sherwood number have been calculated numerically and discussed. Other physical parameters involved in the problem, i.e., Reynolds number Re, Casson fluid parameter $\beta_1$, Prandtl number Pr, Lewis number *Le*, Brownian motion parameter $N_b$, and thermophoresis parameter $N_t$ have been illustrated. The skin friction effect and its physical appearance are also included in this work. The convergence is checked by plotting h-curves. The emerging parameters are discussed by plotting graphs. The recent work is also compared with the published work.

**Keywords:** thin film spray, Casson nanofluid, stretched cylinder, heat and mass transfer, thermophoresis, HAM

## 1. Introduction

The relation among pressure and flow is an important phenomena which plays a vital role to understand the circulation of the blood in the human body and its sustainability. The approach of pressure [1] can bring a partial barrier in some areas of the smaller vessels due to the

IntechOpen

© 2018 The Author(s). Licensee IntechOpen. This chapter is distributed under the terms of the Creative Commons Attribution License (http://creativecommons.org/licenses/by/3.0), which permits unrestricted use, distribution, and reproduction in any medium, provided the original work is properly cited. CC BY

thrilling change of the yield stress. The blood is equally a mixture of two fluids Casson and the other one is Newtonian fluid and studied by Srivastava and Saxena [2]. They focused on the effect of resistance created by the viscosity term and wall shear stresses. Later on, this fluid is studied by many researchers on the stretching surfaces for other industrial and engineering usages [3]. Mahdy [4] have examined the fluid motion over an extending cylinder considering Casson fluid. Hayat et al. [5] have examined the third-order fluid motion over an extending tube within the effect of MHD. Qasim et al. [6] have considered the slip flow of sighted ferrofluid over an extending cylinder. Sheikholeslami [7] has studied the suction idea considering nanofluid over an extended cylinder. Manjunatha et al. [8] have examined the radiation effect in a porous space using dusty fluid and stretching cylinder. Abdulhameed et al. [9] have examined the oscillatory flow phenomena using circular cylinder. Hakeem et al. [10] have studied the flow of Walter's B fluid over an extending sheet. Pandey et al. [11] have studied the Walter's B viscoelastic nanofluid film energetic from below. The interesting and fruitful applications of thin film are the wire and fiber coating, processing of food stuff, extrusion of polymer and metal, drawing of plastic sheets, continuous casting, fluidization of reactor, and chemical processing equipment. On the basis of these applications, researchers did a lot of work on it. Wang [12] was the main researcher who investigated liquid film on an unstable extending surface. Recently Tawade et al. [13] have investigated liquid film flow over an unstable extending surface with thermal radiation, in the existence of continuous magnetic field using numerical method. The liquid film flow considering non-Newtonian fluids proliferates in many life geographies which is used mostly in cylindrical shapes. Several researchers [14–17] investigated power-law fluid with unsteady extending surface using different cases. Megahe [18] and Abolbashari et al. [19] have scrutinized thin film flow of Casson fluid using slip boundary conditions. Recently Qasim et al. [20] have examined the liquid film flow of nanofluid considering Buongiorno's model.

The liquid film spray on a stretching sheet has also an important phenomena to coat the metals and increase their life. The idea of spray on the stretching surface is the study of Wang [21]. Recently Noor et al. [22] considered the thin film spray of nanofluid on a stretching cylinder. They compared their results with the experimental data and found the impact of the physical parameters during flow phenomena. They also discussed the application of their work in detail. Most of the mathematical problems in the field of engineering are composite in their nature, and the exact resolution is very tough or even not conceivable. The solution of these problems is tackled through numerical and analytical methods. Homotopy analysis method is one of the popular techniques for the solution of such complex problems. Liao [22–26] investigates this series solution technique for the solution of nonlinear problems. The other important feature of this method is that its solution contains all the embedded parameters involved in the problem and also the range of the embedded parameters. The high nonlinear problems have been solved by Abbasbandy [27] due to the fast convergence of this method. Alshomrani and Gul [28], Gul [29] have studied the solution of nonlinear differential equations through HAM arises in the field of engineering and industry.

## 2. Formulation

Consider the thin film flow of Casson nanofluid elegantly through a circular cylinder of radius "a." The cylinder is supposed to be stretched along with radial direction with velocity $U_w$, and

temperature at the surface of cylinder is taken $T_w$. The uniform ambient temperature is considered $T_b$ such that $T_w - T_b > 0$ for assisting flow and $T_w - T_b < 0$ for opposing flow.

The governing equations of continuity, heat transfer, and mass transfer are

$$\frac{\partial u}{\partial r} + \frac{u}{r} + \frac{\partial w}{\partial z} = 0, \tag{1}$$

$$u\frac{\partial w}{\partial r} + w\frac{\partial w}{\partial z} = \upsilon\left(1 + \frac{1}{\beta_1}\right)\left(\frac{\partial^2 w}{\partial r^2} + \frac{1}{r}\frac{\partial w}{\partial r}\right) + g\beta^*(T - T_b)(1 - C_b) + \frac{1}{\rho}(\rho^* - \rho)(C - C_b), \tag{2}$$

$$u\frac{\partial u}{\partial r} + w\frac{\partial u}{\partial z} = -\frac{1}{\rho}\frac{\partial P}{\partial r} + \upsilon\left(1 + \frac{1}{\beta_1}\right)\left(\frac{\partial^2 u}{\partial r^2} + \frac{1}{r}\frac{\partial u}{\partial r} - \frac{u}{r^2}\right), \tag{3}$$

$$u\frac{\partial T}{\partial r} + w\frac{\partial T}{\partial z} = \alpha\left(\frac{\partial^2 T}{\partial r^2} + \frac{1}{r}\frac{\partial T}{\partial r}\right) + \frac{\rho^* c_p^*}{\rho c_p}\left(D_B\frac{\partial T}{\partial r}\frac{\partial \phi}{\partial r} + \frac{D_T}{T_b}\left(\frac{\partial T}{\partial r}\right)^2\right), \tag{4}$$

$$u\frac{\partial C}{\partial r} + w\frac{\partial C}{\partial z} = D_B\left(\frac{\partial^2 C}{\partial r^2} + \frac{1}{r}\frac{\partial C}{\partial r}\right) + \frac{D_T}{T_b}\left(\frac{\partial^2 T}{\partial r^2} + \frac{1}{r}\frac{\partial T}{\partial r}\right), \tag{5}$$

where $u(r, z)$ and $w(r, z)$ are velocity components; $\rho$ is density; $\upsilon$ is kinematic viscosity; $\beta_1$ is the constant characteristic to Casson fluid; $\beta^*$ is the coefficient of thermal expansion; $g$ is the gravitational acceleration along z-axis; $T, T_b, C$ and $C_b$ determine the temperature, ambient temperature, concentration, and ambient concentration, respectively; and $\alpha, D_T, D_B$ stands for the thermal diffusivity, thermophoresis diffusion coefficient, and Brownian diffusion coefficient.

The suitable boundary conditions are

$$u = U_w, w = W_w, T = T_w, C = C_w \quad at \quad r = a, \tag{6}$$

$$\mu\frac{\partial w}{\partial r} = \frac{\partial T}{\partial r} = \frac{\partial C}{\partial r} = 0, u = w\frac{d\delta}{dz} \quad at \quad r = b. \tag{7}$$

Here $U_w = -ca$ represents the suction and injection velocity, and $W_w = 2cz$ is the stretching velocity such that $c$ represents the stretching parameter and $\delta$ is the thickness of fluid film.

The similarity transformations are used to alter the basic Eqs. (1)–(7) used in [22] as

$$u = -ca\frac{f(\eta)}{\sqrt{\eta}}, w = 2cz\ \frac{df}{d\eta}, T(z) = T_b - T_{ref}\left(\frac{cz^2}{\upsilon_{nf}}\right)\theta(\eta), C(z) = C_b - C_{ref}\left(\frac{cz^2}{\upsilon_{nf}}\right)\phi(\eta), \tag{8}$$

where

$$\eta = \left(\frac{r}{a}\right)^2.$$

In the case of the outer radius $b$ of the flow, $\eta = \left(\frac{b}{a}\right)^2$.

Using these transformations in Eqs. (1), (2), (4)–(7), we obtained a set of dimensionless equations which is

$$\left(1+\frac{1}{\beta_1}\right)\left(\eta\frac{\partial^3 f}{\partial\eta^3}+\frac{\partial^2 f}{\partial\eta^2}\right)+\mathrm{Re}\left(f\frac{\partial^2 f}{\partial\eta^2}-\left(\frac{\partial f}{\partial\eta}\right)^2+\lambda\left(\theta+Nr\phi\right)\right)=0, \tag{9}$$

$$\eta\frac{\partial^2\theta}{\partial\eta^2}+\frac{\partial\theta}{\partial\eta}+\mathrm{Pr.Re}\left(f\frac{\partial\theta}{\partial\eta}-2\frac{\partial f}{\partial\eta}\theta\right)+\eta\frac{\partial\theta}{\partial\eta}\left(N_t\frac{\partial\theta}{\partial\eta}+N_b\frac{\partial\phi}{\partial\eta}\right)=0, \tag{10}$$

$$\eta\frac{\partial^2\phi}{\partial\eta^2}+\frac{\partial\phi}{\partial\eta}+Le.\mathrm{Re}\left(f\frac{\partial\phi}{\partial\eta}-2\frac{\partial f}{\partial\eta}\phi\right)+\frac{N_t}{N_b}\left(\eta\frac{\partial^2\theta}{\partial\eta^2}+\frac{\partial\theta}{\partial\eta}\right)=0, \tag{11}$$

where

$$\begin{aligned}&\mathrm{Re}=\frac{ca^2}{2\upsilon_{nf}},\ \lambda=\frac{g\beta^*a(T_w-T_\infty)(1-C_\infty)}{W_w^2},\ Nr=\frac{(\rho-\rho^*)(C_w-C_\infty)}{\rho\beta^*(T_w-T_\infty)(1-C_\infty)},\\&\mathrm{Pr}=\frac{\mu c_p}{k},\ N_t=\frac{\rho^*c_p^*D_T\Delta T}{\rho c_p\alpha T_b},\ Le=\frac{\upsilon}{D_B},\ N_b=\frac{\rho^*c_p^*D_B\Delta C}{\rho c_p\alpha}.\end{aligned} \tag{12}$$

In Eq. (12) Re stands for the Reynolds number, $\lambda$ is the buoyancy parameter or in other word it is the natural convection parameter, $Nr$ stands for the buoyancy ratio, Pr represents the Prandtl number, $N_t$ is used to represent thermophoresis parameter, $Le$ is Lewis number, and $N_b$ is Brownian motion parameter.

Physical conditions for momentum, thermal, and concentration fields are transformed as

$$f(1)=\frac{\partial f(1)}{\partial\eta}=\theta(1)=\phi(1)=1, \tag{13}$$

$$\frac{\partial^2 f(\beta)}{\partial\eta^2}=f(\beta)=\frac{\partial\theta(\beta)}{\partial\eta}=\frac{\partial\phi(\beta)}{\partial\eta}=0, \tag{14}$$

where $\beta$ is the thickness of liquid film sprayed on the outer surface of the cylinder.

Integrating Eq. (3) for pressure term

$$\frac{p-p_b}{\mu c}=\frac{\mathrm{Re}}{\eta}f^2-2\left(1+\frac{1}{\beta_1}\right)\frac{\partial f}{\partial\eta}. \tag{15}$$

At the outer surface, the shear stress of the liquid film is zero, i.e.,

$$\frac{\partial^2 f(\beta)}{\partial\eta^2}=0. \tag{16}$$

The shear stress on the cylinder is

$$\tau=\frac{\rho\upsilon 4cz}{a}f''(1)=\frac{4c\mu z}{a}f''(1) \tag{17}$$

The deposition velocity $V$ is written as

$$-V = -ca\frac{f'(\beta)}{\sqrt{\beta}}. \tag{18}$$

Mass flux $m_1$ is in association with the deposition per axial length which is

$$m_1 = V2\pi b \tag{19}$$

The normalized mass flux $m_2$ is

$$m_2 = \frac{m_1}{2\pi a^2 c} = \frac{m_1}{4\pi \upsilon_{nf} \mathrm{Re}} = f(\beta) \tag{20}$$

The flow, temperature, and concentration rates are

$$S_f = \frac{2\upsilon_{nf}}{W_w}\left(\frac{\partial w}{\partial r}\right)_{r=a}, Nu = -\frac{ak}{(T_w - T_b)}\left(\frac{\partial T}{\partial r}\right)_{r=a}, Sh = -\frac{a}{2(C_w - C_b)}\left(\frac{\partial C}{\partial r}\right)_{r=a}. \tag{21}$$

The nondimensional forms for the abovementioned physical properties are

$$\frac{z\mathrm{Re}}{a}S_f = \frac{\partial^2 f(1)}{\partial \eta^2}, Nu = -2k\frac{\partial \theta(1)}{\partial \eta}, Sh = -\frac{\partial \phi(1)}{\partial \eta}. \tag{22}$$

## 3. Solution by homotopy analysis method

Initially guessed values for $f$, $\theta$, and $\phi$ at $\eta = 1$ are

$$\begin{aligned} f_0(\eta) &= \frac{\beta}{2(\beta-1)^3}\left[\eta^3 - 3\beta\eta^2 - (3-6\beta)\eta + (2-3\beta)\right] + \eta, \\ \theta_0(\eta) &= \frac{-\eta^2}{2} + \beta(\eta - 1) + \frac{3}{2}, \phi_0(\eta) = \frac{-\eta^2}{2} + \beta(\eta - 1) + \frac{3}{2}. \end{aligned} \tag{23}$$

The linear operators for the given functions $L_f$, $L_\theta$ and $L_\phi$ are selected as

$$L_f = \frac{\partial^4 f}{\partial \eta^4}, \quad L_\theta = \frac{\partial^2 \theta}{\partial \eta^2} \quad \text{and} \quad L_\phi = \frac{\partial^2 \phi}{\partial \eta^2}, \tag{24}$$

which satisfies the following general solution:

$$L_f\left(A_1 + A_2\eta + A_3\eta^2 + A_4\eta^3\right) = 0, \quad L_\theta(A_5 + A_6\eta) = 0 \quad \text{and} \quad L_\phi(A_7 + A_8\eta) = 0, \tag{25}$$

where $A_i (i = 1 - 8)$ are constants of general solution.

The corresponding nonlinear operators $N_f$, $N_\theta$, and $N_\phi$ are defined as

$$N_f[f(\xi;p),\theta(\xi;p)] = \left(1+\frac{1}{\beta_1}\right)\left(\eta\frac{\partial^3 f(\eta;p)}{\partial\eta^3}+\frac{\partial^2 f(\eta;p)}{\partial\eta^2}\right) + \mathrm{Re}\left(f(\eta;p)\frac{\partial^2 f(\eta;p)}{\partial\eta^2}-\left(\frac{\partial f(\eta;p)}{\partial\eta}\right)^2\right)+\left(\lambda\theta(\eta;p)+Nr\phi(\eta;p)\right)=0, \tag{26}$$

$$N_\theta[f(\xi;p),\theta(\xi;p)] = \eta\frac{\partial^2\theta(\eta;p)}{\partial\eta^2}+\frac{\partial\theta(\eta;p)}{\partial\eta}+\mathrm{Pr.Re}\left(f(\eta;p)\frac{\partial\theta(\eta;p)}{\partial\eta}-2\frac{\partial f(\eta;p)}{\partial\eta}\theta(\eta;p)\right) + \eta\frac{\partial\theta(\eta;p)}{\partial\eta}\left(N_t\frac{\partial\theta(\eta;p)}{\partial\eta}+N_b\frac{\partial\phi(\eta;p)}{\partial\eta}\right)=0, \tag{27}$$

$$N_\phi[f(\eta;p),\phi(\eta;p)] = \eta\frac{\partial^2\phi(\eta;p)}{\partial\eta^2}+\frac{\partial\phi(\eta;p)}{\partial\eta}+Le.\mathrm{Re}\left(f(\eta;p)\frac{\partial\phi(\eta;p)}{\partial\eta}-2\frac{\partial f(\eta;p)}{\partial\eta}\phi(\eta;p)\right) + \frac{N_t}{N_b}\left(\eta\frac{\partial^2\theta(\eta;p)}{\partial\eta^2}+\frac{\partial\theta(\eta;p)}{\partial\eta}\right)=0, \tag{28}$$

where $p\in[0,1]$ is embedded parameter.

## 4. Zeroth-order deformation problem

The equations of zeroth-order deformation problem are obtained as

$$(1-p)L_f\left[f(\eta;p)-f_0(\eta)\right]=ph_fN_f[f(\eta;p)], \tag{29}$$

$$(1-p)L_\theta[\theta(\eta;p)-\theta_0(\eta)]=ph_\theta N_\theta[f(\eta;p),\theta(\eta;p)], \tag{30}$$

$$(1-p)L_\phi\left[\phi(\eta;p)-\phi_0(\eta)\right]=ph_\phi N_\phi\left[f(\eta;p),\phi(\eta;p)\right]. \tag{31}$$

Here $h_f$, $h_\theta$ and $h_\phi$ are auxiliary nonzero parameters. The corresponding boundary conditions are written as

$$f(\eta;p)_{\eta=1}=1,\left.\frac{\partial f(\eta;p)}{\partial\eta}\right|_{\eta=1}=1,\theta(\eta;p)\big|_{\eta=1}=1,\phi(\eta;p)\big|_{\eta=1}=1, \tag{32}$$

$$\left.\frac{\partial^2 f(\eta;p)}{\partial\eta}\right|_{\eta=\beta}=0,\left.\frac{\partial\theta(\eta;p)}{\partial\eta}\right|_{\eta=\beta}=0,\left.\frac{\partial\phi(\eta;p)}{\partial\eta}\right|_{\eta=\beta}=0. \tag{33}$$

Since

$$p=0\Rightarrow f(\eta;0)=f_0(\eta)=\eta,\theta(\eta;0)=\theta_0(\eta)=1,\phi(\eta;0)=\phi_0(\eta)=1, \tag{34}$$

$$p = 1 \Rightarrow f(\eta;1) = f(\eta), \theta(\eta;1) = \theta(\eta), \phi(\eta;1) = \phi(\eta). \tag{35}$$

Using the Taylor's expansions of $f(\eta;p)$, $\theta(\eta;p)$ and $\phi(\eta;p)$ about $p = 0$ in Eqs. (28)–(31), we obtained

$$f(\eta;p) = f_0(\eta) + \sum_{w=1}^{\infty} f_w(\eta) p^w, \tag{36}$$

$$\theta(\eta;p) = \theta_0(\eta) + \sum_{w=1}^{\infty} \theta_w(\eta) p^w, \tag{37}$$

$$\phi(\eta;p) = \phi_0(\eta) + \sum_{w=1}^{\infty} \phi_w(\eta) p^w, \tag{38}$$

where

$$f_w(\eta) = \frac{1}{w!} \frac{\partial^w f\ (\eta;p)}{\partial \eta^w}\bigg|_{p=0}, \theta_w(\eta) = \frac{1}{w!} \frac{\partial^w \theta\ (\eta;p)}{\partial \eta^w}\bigg|_{p=0}, \phi_w(\eta) = \frac{1}{w!} \frac{\partial^w \phi\ (\eta;p)}{\partial \eta^w}\bigg|_{p=0}. \tag{39}$$

The convergence of series depends on $h_f$, $h_\theta$, and $h_\varphi$. So let us suppose that series converges at $p = 1$ for some values of $h_f$, $h_\theta$, and $h_\varphi$, then Eqs. (35)–(37) become

$$f(\eta) = f_0(\eta) + \sum_{w=1}^{\infty} f_w(\eta), \tag{40}$$

$$\theta(\eta) = \theta_0(\eta) + \sum_{w=1}^{\infty} \theta_w(\eta), \tag{41}$$

$$\phi(\eta) = \phi_0(\eta) + \sum_{w=1}^{\infty} \phi_w(\eta). \tag{42}$$

## 5. $w^{th}$ order deformation problem

By taking $w$ times derivatives of Eqs. (28)–(32) and then dividing by $w!$ as well as substituting $p = 0$, we obtained the following equations:

$$L_f\left[f_w(\eta) - \chi_w f_{w-1}(\eta)\right] = \hbar_f\ \Re_w^f(\eta), \tag{43}$$

$$L_\theta[\theta_w(\eta) - \chi_w \theta_{w-1}(\eta)] = \hbar_\theta\ \Re_w^f(\eta), \tag{44}$$

$$L_\phi\left[\phi_w(\eta) - \chi_w \phi_{w-1}(\eta)\right] = \hbar_\phi\ \Re_w^f(\eta), \tag{45}$$

where

$$\chi_w = \begin{cases} 0, & \text{if} \quad p \leq 1 \\ 1, & \text{if} \quad p > 1 \end{cases}.$$

$$\Re_w^f(\eta) = \left(1 + \frac{1}{\beta_1}\right)\left(\eta f'''_{w-1} + f''_{w-1}\right) + \mathrm{Re}\sum_{j=0}^{w-1}\left(f_{w-1-j} f''_j - f'_{w-1-j} f'_j\right) + \left(Gr_t \theta_{w-1} + Gr_c \phi_{w-1}\right), \tag{46}$$

$$\Re_w^\theta(\eta) = \eta\theta''_{w-1} + \theta'_{w-1} + \mathrm{Pr.Re}\sum_{j=0}^{w-1}\left(f_{w-1-j}\theta'_j - 2f'_{w-1-j}\theta_j\right) + \eta\theta'_{w-1}\sum_{j=0}^{w-1}\left(N_t\theta'_{w-1} + N_b\phi'_{w-1}\right), \tag{47}$$

$$\Re_w^\phi(\eta) = \eta\phi''_{w-1} + \phi'_{w-1} + Le.\mathrm{Re}\sum_{j=0}^{w-1}\left(f_{w-1-j}\phi'_j - 2f'_{w-1-j}\phi_j\right) + \frac{N_t}{N_b}\left(\eta\theta''_{w-1} + \theta'_{w-1}\right). \tag{48}$$

The related boundary conditions are

$$\begin{aligned} f_w(1) = f'_w(1) = \theta_w(1) = \phi_w(1) = 1, \\ f''_w(\beta) = \theta'_w(\beta) = \phi'_w(\beta) = 0. \end{aligned} \tag{49}$$

The general solution of Eqs. (42)–(44) is given by

$$\begin{aligned} f_w(\eta) &= e_1 + e_2\eta + e_3\eta^2 + f_w^*(\eta), \\ \theta_w(\eta) &= e_4 + e_5\eta + \theta_w^*(\eta), \\ \phi_w(\eta) &= e_6 + e_7\eta + \phi_w^*(\eta). \end{aligned} \tag{50}$$

Here $f_w^*(\xi)$, $g_w^*(\xi)$ and $\theta_w^*(\xi)$ represent the particular solutions, and the constant $A_i (i = 1 - 8)$ are determined from boundary conditions (49).

## 6. Discussion about graphical results

The purpose of this study is to enhance the heat and mass diffusion by choosing a thin-layer spray of the Casson nanofluid over a stretching cylinder. The physical configuration of the problem is shown in **Figure 1**. The solution of the problem has been obtained using the homotopy approach, and the main features for the convergence (h-curves) of homotopy analysis method (HAM) have been shown in **Figures 2** and **3**. These figures demonstrate the h-curves for velocity, temperature, and concentration fields, respectively. The impact of buoyancy parameter $\lambda$ and buoyancy ratio $Nr$ on velocity field is prescribed in **Figure 4**. Velocity grows with the rising values of $\lambda$ because the natural convection parameter $\lambda$ and momentum boundary layer are in direct relation. The similar effect for the rising values of $N_r$ can be seen in **Figure 4**. The effect of thickness parameter $\beta$ and Casson fluid parameter $\beta_1$ versus velocity field is shown in **Figure 5**. Increasing values of $\beta$ generate friction force and decline the velocity field because the thicker flow creates hurdles in fluid motion, while the thin layer is comparatively fast flowing.

http://dx.doi.org/10.5772/intechopen.79772

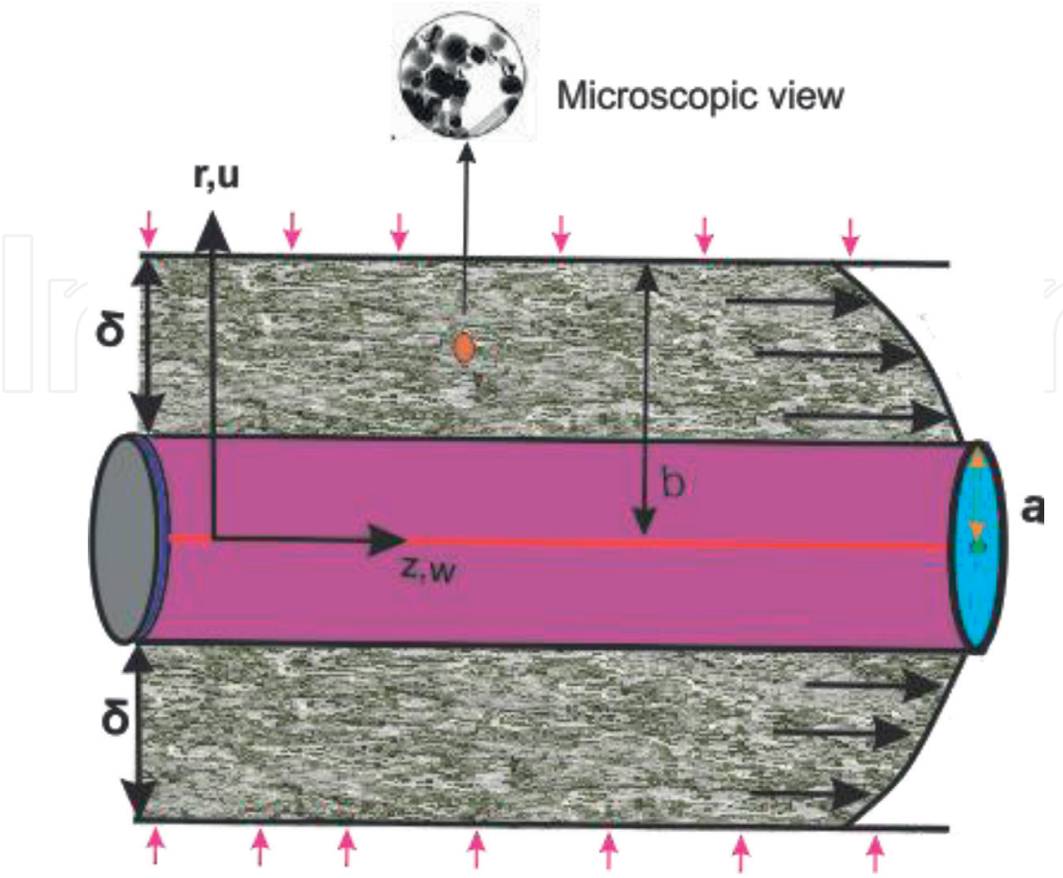



**Figure 1.** Physical geometry of the problem.

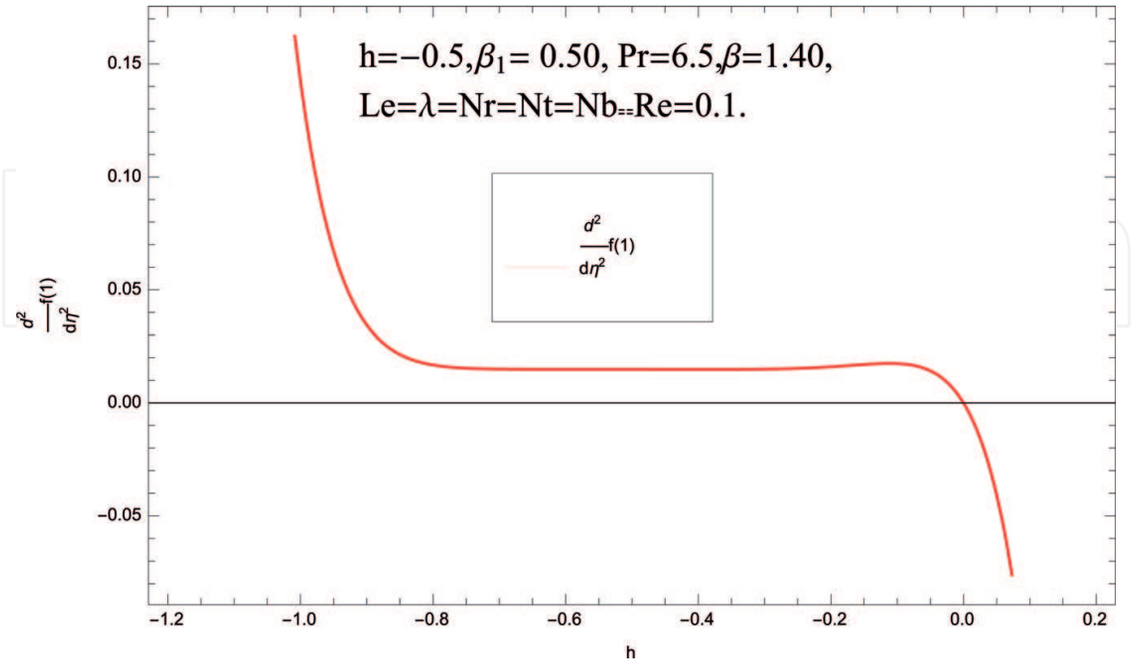



**Figure 2.** h-curve for velocity profile.

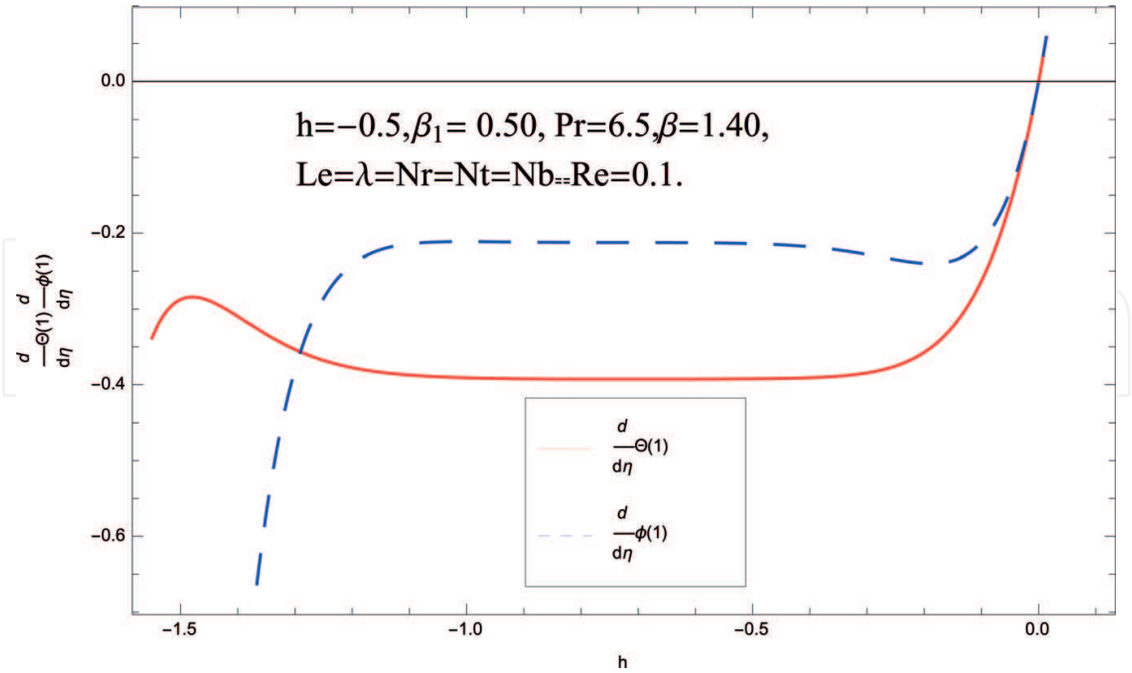



**Figure 3.** Combined h-curve for temperature and concentration fields.

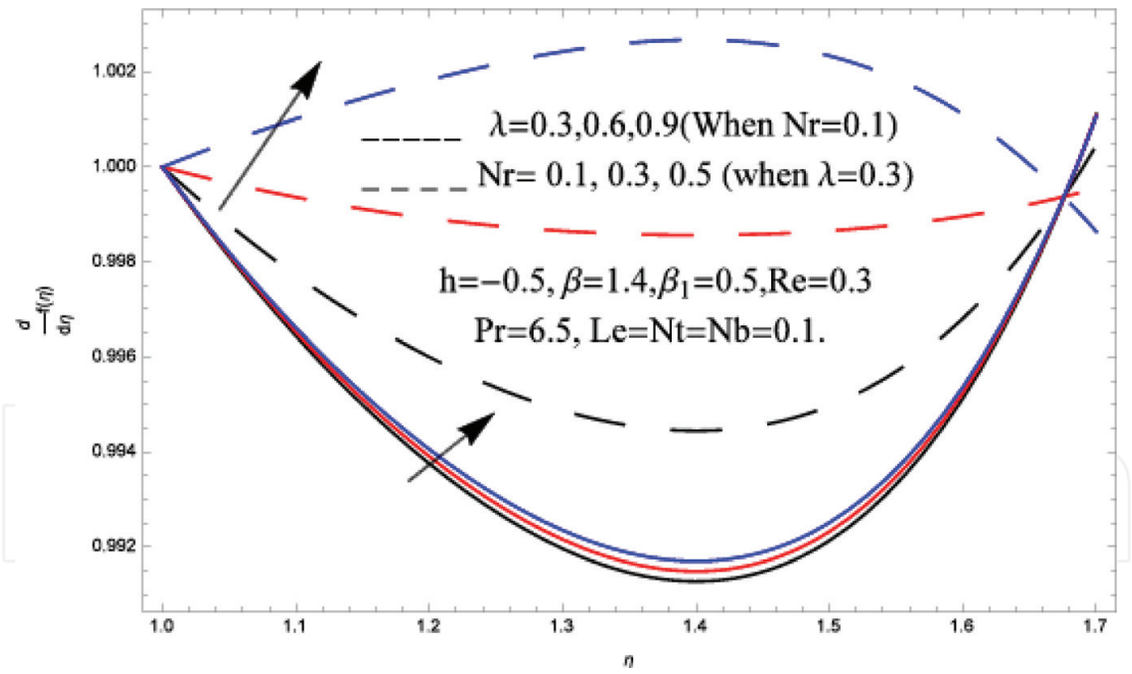



**Figure 4.** Variation of velocity with $Nr$ and $\lambda$.

Therefore, larger amount of $\beta$ declines the flow motion. The similar effect of the larger amount of the Casson fluid parameter $\beta_1$ is shown in **Figure 5**. The rising values of the parameter $\beta_1$ imply a decline in the yield stress of the Casson fluid. In **Figure 6**, the behavior of the thermophoretic parameter $N_t$ and Reynolds number Re is observed over the field of temperature.

http://dx.doi.org/10.5772/intechopen.79772

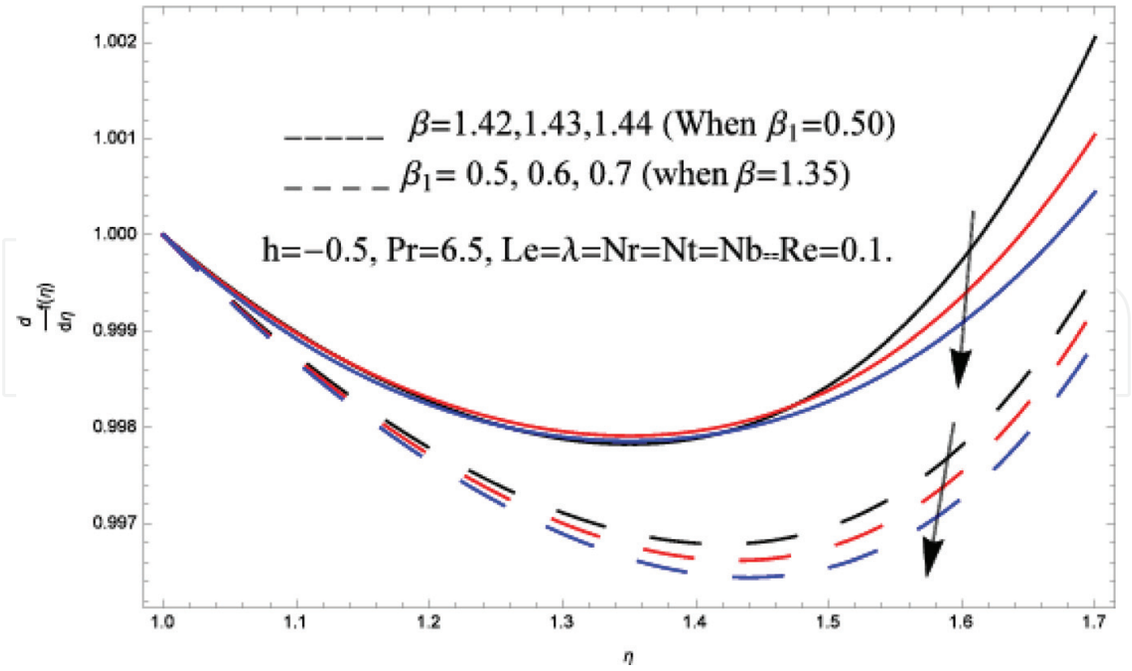



**Figure 5.** Variation of velocity with $\beta$ and $\beta_1$.

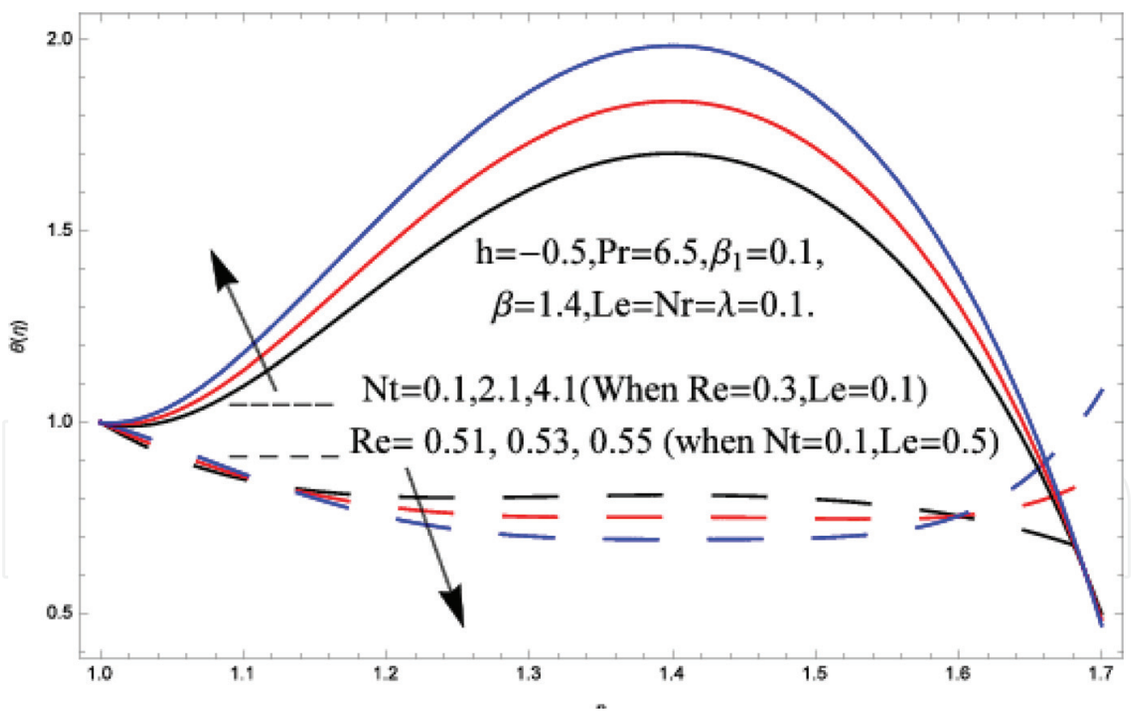



**Figure 6.** Variation of *Nt* and Re.

The larger amount of thermophoresis parameter $N_t$ depreciates temperature profile because rising values of $N_t$ enhance the concentration profile due to its direct relation and its product in the model equation increases the cooling effect to reduce the temperature field. The larger quantity of Re reduces temperature field. Rising values of Reynolds number Re enhance the

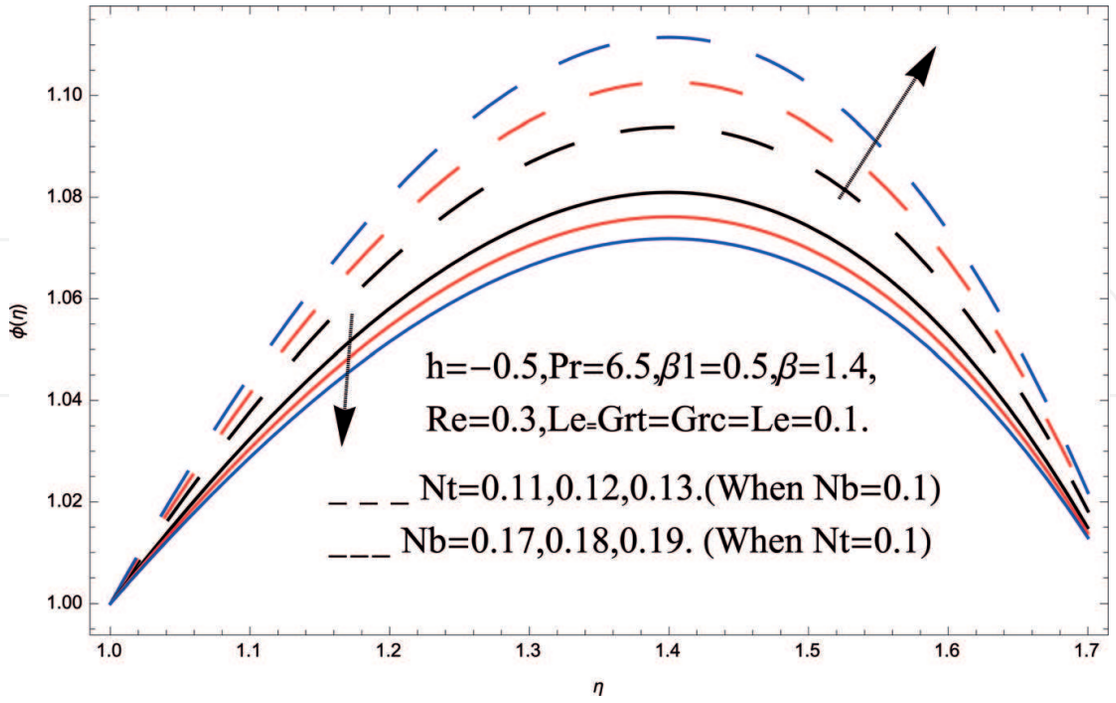



**Figure 7.** Variation of *Nt* and *Nb*.

inertial forces. The powerful inertial forces kept the fluid particles tightly closed, and more heat energy is required to break down the bonds among these atoms. In other words the inertial forces raise the boiling point of the fluid, and more heat energy is required to enhance the temperature. **Figure 7** shows the influences of thermophoretic parameter $N_t$ and Brownian motion parameter $N_b$ in concentration field. The larger amount of $N_b$ displays a falling performance against concentration field. The parameter $N_b$ is owing to the thinning of boundary layer because the random flow of liquid particles makes the decline in the concentration. The rising values of thermophoresis parameter $N_t$ enhance the concentration field. The reason behind this is that $N_t$ is in direct relation with concentration pitch, while the $N_b$ is in inverse relation to the concentration field.

**Figure 8** represents the behavior of the concentration field with respect to Reynolds number Re and Lewis number *Le*. The larger amount of Re improves the concentration field. The reason is that larger values of Re generate the enhancement in the inertial forces to rise concentration field. The concentration boundary layer is falling with the rising value of Lewis number *Le*.

**Figure 9** shows the relationship between pressure distribution over the stretching surface versus Reynolds number Re and Casson fluid parameter $\beta_1$. The larger amount of $\beta_1$ increases the viscous forces, and more pressure are required at the surface. Thus the larger amount of $\beta_1$ decreases the pressure distribution. The larger amount of the Reynolds number Re decreases the pressure distribution. The strong inertial effects packed the fluid particle tightly, and as a result the pressure distribution decreases.

**Table 1** shows the numerical values of the skin friction coefficient, local Nusselt number, and Sherwood number of various physical parameters. The skin friction coefficient rises with the

http://dx.doi.org/10.5772/intechopen.79772

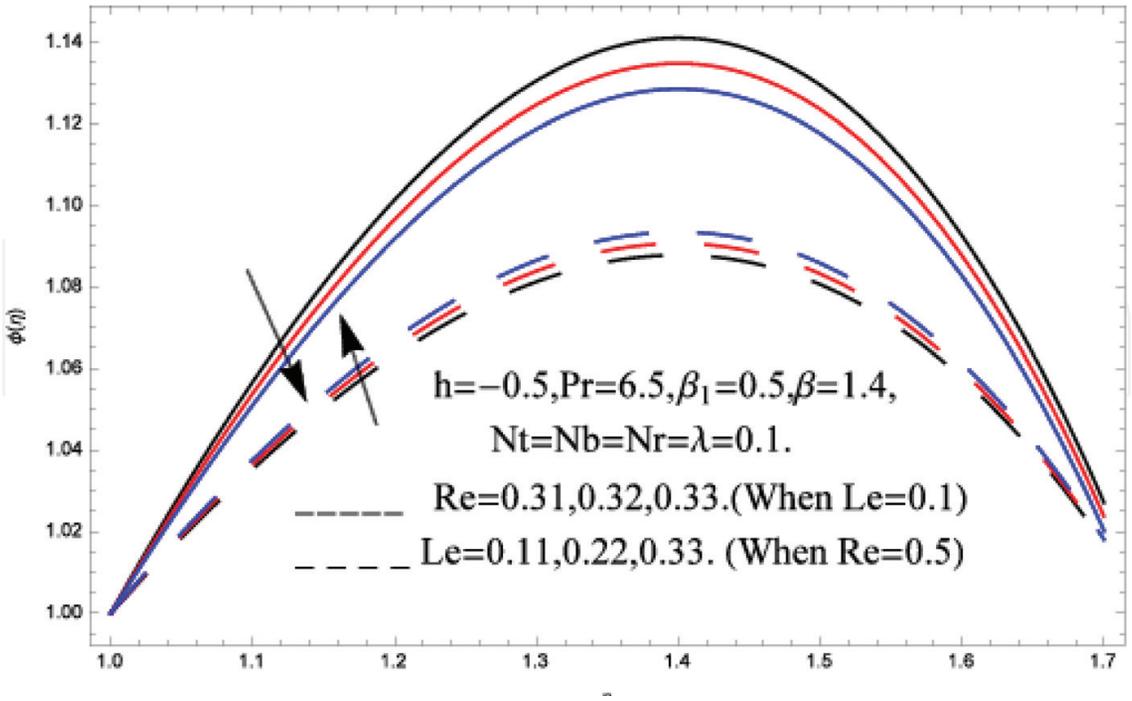



**Figure 8.** Variation of Re and *Le*.

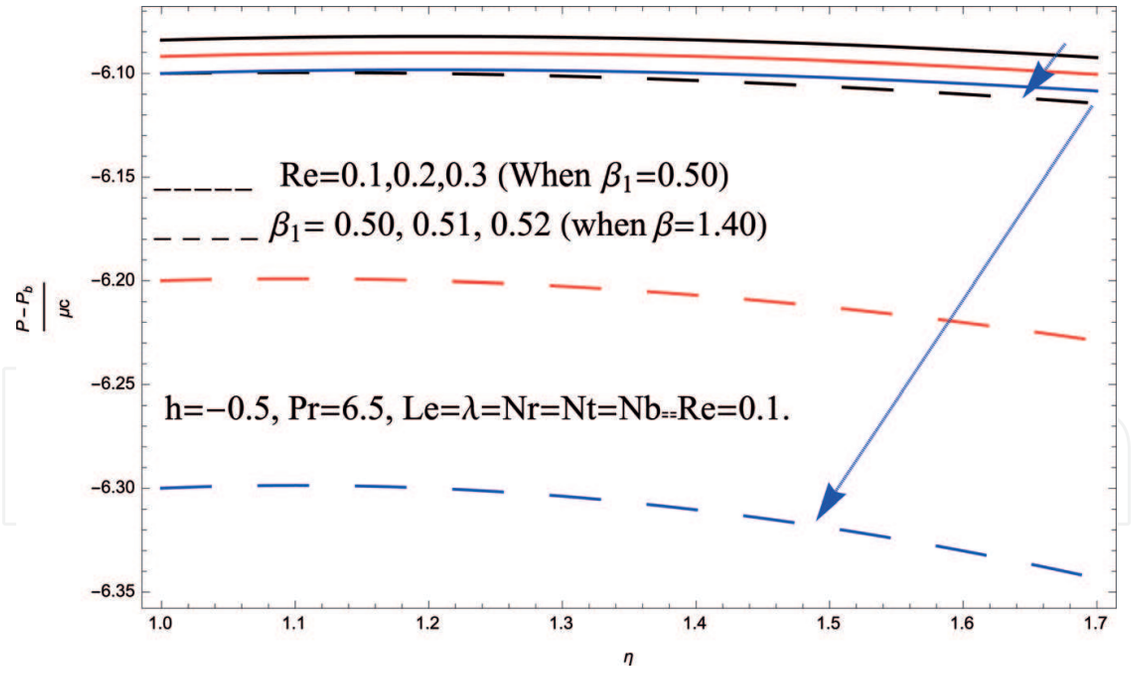



**Figure 9.** Variation of pressure term.

growth of thickness parameter $\beta$. The thick boundary layer increases friction force and improves the cooling effect. Therefore, the Nussselt and Sherwood numbers are increased. The Reynolds number Re decreases the fluid flow due to inertial forces. Due to this reason, the larger quantity of Re enhances the $f''(1), \Theta'(1)$ and $\phi'(1)$. Similar effect for rising values of the

| $\beta$ | Re | $\beta_1$ | $f''(1)$ | $\theta'(1)$ | $\phi'(1)$ |
|---|---|---|---|---|---|
| 1.5 | 0.8 | 1.2 | 0.0149342 | 0.785646 | 0.212503 |
| 1.6 | | | 0.0150964 | 0.916634 | 0.260143 |
| 1.7 | | | 0.01673959 | 1.03338 | 0.309284 |
| | 0.8 | | 0.0149342 | 0.785646 | 0.212503 |
| | 0.9 | | 0.0151422 | 0.881567 | 0.240775 |
| | 1.0 | | 0.0149653 | 0.976928 | 0.269410 |
| | | 1.2 | 0.0149342 | 0.785646 | 0.212503 |
| | | 1.3 | 0.0154906 | 0.785691 | 0.212518 |
| | | 1.4 | 0.0160015 | 0.785733 | 0.212531 |

**Table 1.** Numerical values for skin friction coefficient, local Nusselt number, and Sherwood number for various physical parameters when $h = -0.5, Pr = 0.5, \beta_1 = 1.2, \beta = 1.5, Nt = 0.5, Nb = 1, Nr = 0.6, \mathrm{Re} = 0.8, Le = 0.5$.

| Re | [30] | [31] | [4] | Present |
|---|---|---|---|---|
| 0.5 | 0.88220 | 0.8827 | 0.88691 | 0.886942 |
| 1.0 | 1.17776 | 1.1781 | 1.17953 | 1.72926 |
| 2.0 | 1.59390 | 1.5941 | 1.59434 | 3.26714 |
| 5.0 | 2.41745 | 2.4175 | 2.4175 | 6.75053 |
| 10.0 | 3.34445 | 3.3445 | 3.34447 | 10.1078 |

**Table 2.** Values of $f''(1)$ for various Reynolds numbers when $h = -0.5, Pr = 0.5, \beta_1 = 1.2, \beta = 1.1, Nt = 0.5, Nb = 1, Nr = 0.6, Le = 0.5$.

| Pr | [30] | [31] | [4] | Present |
|---|---|---|---|---|
| 0.7 | 1.568 | 1.5683 | 1.56878 | 1.56846 |
| 2.0 | 3.035 | 3.0360 | 3.03596 | 3.68121 |
| 7.0 | 6.160 | 6.1592 | 6.15813 | 7.24452 |
| 10.0 | 10.77 | 7.4668 | 7.46477 | 10.2634 |

**Table 3.** Values of $-\theta'(1)$ for various Prandtl numbers when $h = -0.5, \beta_1 = 1.2, \beta = 1.1, Nt = 0.5, Nb = 1, Nr = 0.6, \mathrm{Re} = 0.8, Le = 0.5$.

Casson parameter $\beta_1$ has been shown in **Table 1**. The reason is that the viscous forces become dominant with the larger amount of $\beta_1$ to enhance the $f''(1)$, $\Theta'(1)$ and $\phi'(1)$. The comparison of present work and published work has been shown in **Tables 2** and **3**, and closed agreement for $f''(1)$, $\Theta'(1)$ and $\phi'(1)$ has been achieved.

## 7. Conclusion

The heat and mass transfer effect of a thin film over the extended surface of a cylinder has been explored in the recent research. The spray phenomenon has been studied in the form of

velocity, temperature, concentration, and pressure distribution profiles, respectively. The similarity transformation has been used to alter the governing equations into the set of nonlinear differential equations. The solution of the problems has been obtained through the homotopy analysis method (HAM). The impact of the embedded parameters has been examined and discussed. The outcomes of the recent study have been pointed out as:

- The inertial forces become stronger with the larger amount of Reynolds number Re, and as a result the velocity of the fluid flow reduces, while the upsurge values of Reenhance the $f''(1)$. Similarly, the Nusselt number and the Sherwood number are also increasing.
- The larger amount of the thickness parameter $\beta$ of the thin film produces hurdles in the spray phenomenon, and as a result the velocity of the fluid decreases. On the other hand, the skin friction, Nusselt number, and the Sherwood number grow with the larger values of $\beta$. In fact, the cooling effect increases with the rising values of $\beta$ to enhance the friction force.
- The greater amount of the Brownian motion parameter $N_b$ declines the concentration field. The reason is that the rising values of $N_b$ improve the thinning of the fluid layer and as a result the concentration profile reduces.
- The temperature field increases with the rising value of the thermophoresis parameter $N_t$, while the concentration field falls to reduce with the larger amount of $N_t$, because the thermophoresis parameter is in inverse relation to the concentration profile.
- The comparison of the present study with the published work authenticates the obtained result.

## Author details

Taza Gul[1,2]* and Shakeela Afridi[1]

*Address all correspondence to: tazagulsafi@yahoo.com

1 Higher Education Department, Khyber Pakhtunkha, Pakistan

2 Department of Mathematics, City University of Science and Information Technology, Pakistan

## References

[1] Joly L. In: Copley, editor. Hemorheology. New York: Pergamon Press; 1967. pp. 1-41

[2] Srivastava VP, Saxena M. Two-layered model of casson fluid flow through stenotic blood vessels: Application to the cardiovascular system. Journal of Biomechanics. 1994;**11**:921-928

[3] Pramanik S. Casson fluid flow and heat transfer past an exponentially porous stretching surface in presence of thermal radiation. Ain Shams Engineering Journal. 2014;**5**:205-212

[4] Mahdy A. Heat transfer and flow of a casson fluid due to a stretching cylinder with the Soret and Dufour effects. Journal of Engineering Physics and Thermophysics. 2015;**88**:928-936

[5] Hayat T, Shafiq A, Alsaedi A. MHD axisymmetric flow of third grade fluid by a stretching cylinder. Alexandria Engineering Journal. 2015;**54**:205-212

[6] Qasim M, Khan ZH, Khan WA, Shah IA. MHD boundary layer slip flow and heat transfer of ferrofluid along a stretching cylinder with prescribed heat flux. PLoS One. 2014;**9**:1-6

[7] Sheikholeslami M. Effect of uniform suction on nanofluid flow and heat transfer over a cylinder. Journal of the Brazilian Society of Mechanical Sciences and Engineering. 2015;**37**: 1623-1633

[8] Manjunatha PT, Gireesha BJ, Prasannakumara BC. Effect of radiation on flow and heat transfer of MHD dusty fluid over a stretching cylinder embedded in a porous medium in presence of heat Source. International Journal of Applied Computational Science and Mathematics. 2017;**3**:293-310

[9] Abdulhameed M, Vieru D, Sharidan S. Comparison of different pressure waveforms for heat transfer performance of oscillating flow in a circular cylinder. Engineering Science and Technology, an International Journal. 2016;**19**:1040-1049

[10] Hakeem AKA, Ganesh NV, Ganga B. Effect of heat radiation in a Walter's liquid B fluid over a stretching sheet with non-uniform heat source/sink and elastic deformation. Journal of King Saud University—Engineering Sciences. 2014;**26**:168-175

[11] Pandey SD, Nema VK, Tiwari S. Charateristic of Walter's B visco-elastic nanofluid layer heated from below. International Journal of Energy Engineering. 2016;**6**:7-13

[12] Wang CY. Liquid film on an unsteady stretching surface. Quarterly of Applied Mathematics. 1990;**48**:601-610

[13] Tawade L, Abel M, GMetri P, Koti A. Thin film flow and heat transfer over an unsteady stretching sheet with thermal radiation, internal heating in presence of external magnetic field. International Journal of Applied Mathematics and Mechanics. 2016;**3**:29-40

[14] Andersson HI, Aarseth JB, Braud N, Dandapat BS. Flow of a power-law fluid film on an unsteady stretching surface. Journal of Non-Newtonian Fluid Mechanics. 1996;**62**:1-8

[15] Chen CH. Heat transfer in a power-law liquid film over an unsteady stretching sheet. Heat and Mass Transfer. 2003;**39**:791-796

[16] Wang C, Pop L. Analysis of the flow of a power-law liquid film on an unsteady stretching surface by means of homotopy analysis method. Journal of Non-Newtonian Fluid Mechanics. 2006;**138**:161-172

[17] Chen CH. Effect of viscous dissipation on heat transfer in a non-Newtonian liquid film over an unsteady stretching sheet. Journal of Non-Newtonian Fluid Mechanics. 2006;**135**: 128-135

[18] Megahe AM. Effect of slip velocity on Casson thin film flow and heat transfer due to unsteady stretching sheet in presence of variable heat flux and viscous dissipation. Applied Mathematics and Mechanics. 2015;**36**:1273-1284

[19] Abolbashari HM, Freidoonimehr N, Rashidi MM. Analytical modeling of entropy generation for Casson nano-fluid flow induced by a stretching surface. Advanced Powder Technology. 2015;**26**:542-552

[20] Qasim M, Khan ZH, Lopez RJ, Khan WA. Heat and mass transfer in nanofluid thin film over an unsteady stretching sheet using Buongiorno's model. European Physical Journal–Plus. 2016;**131**:1-16

[21] Wang CY. Liquid film sprayed on a stretching cylinder. Chemical Engineering Communications. 2006;**193**:869-878

[22] Noor SK, Gul T, Islam S, Khan I, Aisha MA, Alshomrani AS. Magnetohydrodynamic nanoliquid thin film sprayed on a stretching cylinder with heat transfer. Applied Sciences. 2017;**271**:1-25

[23] Liao SJ. The proposed homotopy analysis method for the solution of nonlinear problems [PhD thesis]. Applied Mathematics and Computation 147 (2004) 499-513. Shangai Jiao Tong Universit; 1992

[24] Liao SJ. An explicit, totally analytic approximate solution for blasius viscous flow problems. International Journal of Non-Linear Mechanics. 1999;**34**:759-778

[25] Liao SJ. Beyond Perturbation: Introduction to the Homotopy Analysis Method. Boca Raton: Chapman and Hall, CRC; 2003

[26] Liao SJ. On the analytic solution of magnetohydrodynamic flows of non-newtonian fluids over a stretching sheet. Journal of Fluid Mechanics. 2003;**488**:189-212

[27] Abbasbandy S. The application of homotopy analysis method to nonlinear equations arising in heat transfer. Physics Letters A. 2006;**360**:109-113

[28] Alshomrani AS, Gul T. The convective study of the $Al_2O_3$-$H_2O$ and Cu-$H_2O$ nano-liquid film sprayed over a stretching cylinder with viscous dissipation. European Physical Journal–Plus. 2017;**132**:495

[29] Gul T. Scattering of a thin layer over a nonlinear radially extending surface with magnetohydrodynamic and thermal dissipation. Surface Review and Letters. 1850123. DOI: 10.1142/S0218625X18501238

[30] Wang CY. Fluid flow due to a stretching cylinder. Physics of Fluids. 1988;**31**:466-468

[31] Ishak A, Nazar R, Pop I. Uniform suction/blowing effect on flow and heat transfer due to a stretching cylinder. Applied Mathematical Modelling. 2008;**32**:2059-2066

IntechOpen

IntechOpen